Moving the pulsed heating technique beyond monolithic specimens: Experiments with coated wires

D. Josell, D. Basak, J.L. McClure, U.R. Kattner, M.E. Williams, and W.J. Boettinger
Metallury Division, National Institute of Standards and Technology, Gaithersburg, Maryland
M. Rappaz
Department of Materials, Ecole Polytechnique Federal Lausanne, Lausanne, Switzerland

(Received 29 January 2001; accepted 5 June 2001)

Pulsed heating experiments that measure high-temperature thermophysical properties using pyrometric measurement of the temperature–time history of metal specimens rapidly heated by passage of electric current have a 30-year history at the National Institute of Standards and Technology. In recent years, efforts have been made to move beyond the limitations of the standard technique of using costly, black-body geometry specimens. Specifically, simultaneous polarimetry measurement of the spectral emissivity has permitted study of sheet and wire specimens. This paper presents the results of two efforts to expand beyond the macroscopically monolithic, single-phase materials of all previous studies. In the first study the melting temperatures of coatings, including Ti and Ti(Al) alloys, deposited on higher melting Mo substrates are measured. In the second study the melting temperatures of substrates, Ti and Cr, covered by higher melting W and Mo coatings are measured.

I. INTRODUCTION

Pulsed heating experiments based on pyrometric and electrical measurement of the temperature–time history of metal specimens rapidly heated by passage of electric current have been used to obtain melting temperatures, specific heats, and latent heats at the National Institute of Standards and Technology (NIST) for the past 30 years.[1,2] Electrical and magnetic issues related to the pulsed current in these experiments are detailed in Ref. 2 in particular; for the currents and pulse times in these experiments, spatial variation of current density due to such effects is negligible. Early experiments utilized tubular specimens with small sighting holes to approximate black-body conditions. The pyrometer is focused on the hole, and the experimentally measured pyrometer voltages can be directly converted to true temperatures without knowledge of the spectral emissivity of the specimen at the pyrometer wavelength. Such experiments provide thermodynamic data for elemental materials at elevated temperatures, with uncertainties in determination of, e.g., melting temperature as small as those associated with the pyrometric determination of temperature, typically approximately 8 K (2σ) at temperatures near 2000 K. A significant drawback of such specially prepared specimens is their cost.

Some recent efforts attempt to move beyond the limitations of this standard technique. Specifically, polarimetric measurement of the spectral emissivity of the specimen surface, concurrent with pyrometric measurement of the radiance temperature on the same surface, has permitted study of sheet and wire specimens[3] rather than costly black-body geometry specimens. Such a technique permitted a study of the impact of heating rate and grain size on the melting behavior exhibited by a Nb–47 mass% Ti alloy.[4] The savings do come with other "costs", specifically loss of accuracy in temperature determination caused by inclusion of an additional real-time measurement (spectral emissivity). However, the accuracy is still significantly higher than that of other experimental techniques, e.g., visual observation of melting. For refractory metals and alloys, where many melting temperatures have uncertainties approaching or exceeding 100 K (see below), the enhanced versatility of such a technique far outweighs the increased uncertainty of the measurements. It is in the spirit of further increasing the versatility of the technique that this paper moves beyond the macroscopically monolithic, single-phase materials of previous studies. All temperatures given in this paper are true temperatures computed using Planck's law and the measured emissivities and radiance temperatures.

Two separate types of experiments are detailed. The first study is of the melting behavior of lower melting coatings, particularly Ti and Ti(Al) alloys, deposited on higher melting Mo substrates. The second study is of the melting behavior of lower melting substrates, particularly Ti and Cr, covered by higher melting Mo or W/Mo

https://doi.org/10.1557/JMR.2001.0332

coatings. In both cases a current of 500–1500 A resistively heats the specimen through the duration of the experiment, typically 50 to 100 ms from the initial application of the current until the inception of melting and subsequent failure. The experiments with the pure Ti as coating or substrate are meant to assess the accuracy of such experiments through comparison of the measured melting temperatures to the known melting temperature of Ti (T_m = 1943 ± 2 K). The experiments with the Ti(Al) coatings subsequently apply the technique to measure melting temperatures of alloy compositions in an industrially relevant binary phase diagram. The experiments with the Cr coated with Mo or W/Mo measure the poorly known melting point of elemental Cr; the high vapor pressure of Cr at temperatures approaching its melting point prevents accurate determination of this temperature by most techniques. Use of both low-oxygen content and high-oxygen content "99.99% (metals basis)" Cr permit evaluation of features on the Cr–O binary phase diagram as well.

II. SPECIMEN PREPARATION

All coatings were deposited by electron beam evaporation. The deposition system has three separate sources and a base pressure of approximately 10^{-6} Pa (10^{-8} torr). Titanium approximately 0.5-μm thick was preevaporated on the walls of the deposition chamber at the start of deposition to eliminate contamination caused by outgassing from the chamber walls. Substrate surfaces were sputter-cleaned using ionized Ar from an *in situ* ion source prior to deposition of the coatings. For deposition of alloys, two sources were run simultaneously. Composition control was based on the individual deposition rates of the two sources as recorded by two quartz crystal monitors. Compositions quoted in this paper are measured compositions, obtained directly from cross sections of the coated specimens using energy dispersive x-ray spectroscopy (EDS) with elemental standards in a scanning electron microscope.

For the Ti(Al) alloy depositions, a flat surface was polished on the side of the Mo rod with length equal to the length of the rod and width approaching the diameter of the rod. Deposits on this flat surface were smoother than those on the curved surface, exhibiting higher reflectivities, which improved the signal to noise of the measurements. The starting Al was 99.99% pure as specified by the manufacturer. The Ti source used for deposition of the coatings was prepared by the iodide process, having a 99.9% stated purity and measured oxygen and nitrogen contents of 10^{-4} at.% (100 ppm) and 10^{-5} at.% (10 ppm), respectively.[5] Additional nitrogen or oxygen pickup during deposition of the coatings cannot be ruled out. Titanium and Ti(Al) coatings were deposited on Mo (99.99%) rods of 1.6-mm diameter (substrates) to study the melting behavior of the coatings. Interdiffusion of Mo into Ti and Ti(Al) only raises the solidus and liquidus temperatures. This ensures that the inception of melting corresponds to that of the pure material rather than that of any interdiffused region.

Microscopy (both optical and scanning electron) of 99.99% (metals basis) Cr used as a substrate material indicated the presence of a second phase located at the grain boundaries. Composition analysis demonstrated that these 1 to 10 μm diameter regions were oxygen rich, with atomic fractions between 46 and 58% Cr, with the remainder oxygen by difference. Such oxides are typical of "high-purity (metals basis)" Cr grown by electrodeposition. With oxide particles approximately 6 μm in diameter spaced approximately 50 μm apart (optical microscopy), this material had an oxide volume fraction of approximately 1% and, thus, an average of approximately 0.005 atomic fraction oxygen. This material is referred to as "high-oxygen" Cr in this paper. Also used as substrate material was Cr of purity 99.95% (metals basis) with 2.5×10^{-4} atomic fraction oxygen (76 ppm by weight determined by the manufacturer); it is referred to as "low-oxygen" Cr. The Cr was coated with W and Mo to study the melting behavior of the Cr substrates. The double W/Mo coating was used to prevent the formation of lower melting compositions by Cr–Mo interdiffusion. No such regions exist in either the Cr–W or W–Mo phase diagrams. The Mo overlayer was used because deposition of a sufficiently thick layer of W alone was impractical. Nitrogen or oxygen pickup during deposition of the coatings is irrelevant since it does not affect the melting point of the Cr substrate material.

III. RESULTS AND DISCUSSION: MELTING OF COATINGS

A. Pure titanium coatings

Specimens were fabricated with 10 μm-thick Ti coatings on Mo rods. Experiments were conducted to determine the heating rates that sufficiently minimized interdiffusion between the coatings and substrate materials. The temperature at which the spectral emissivity exhibited a discontinuous decrease was taken as smoothing of the surface caused by melting.[4] Data from 21 experiments are summarized in Fig. 1. The melting point is independent of heating rate above approximately 1×10^4 K s^{-1}. The increase of melting temperature at slower heating rates is consistent with increased interdiffusion during the longer times associated with these experiments. Such interdiffusion was confirmed by EDS of cross-sectioned specimens obtained from experiments terminated prior to melting of the coating. The melting temperature measured at the highest heating rates (negligible interdiffusion) is approximately 10 K higher than the value of 1945 K obtained in this laboratory using pure

https://doi.org/10.1557/JMR.2001.0332

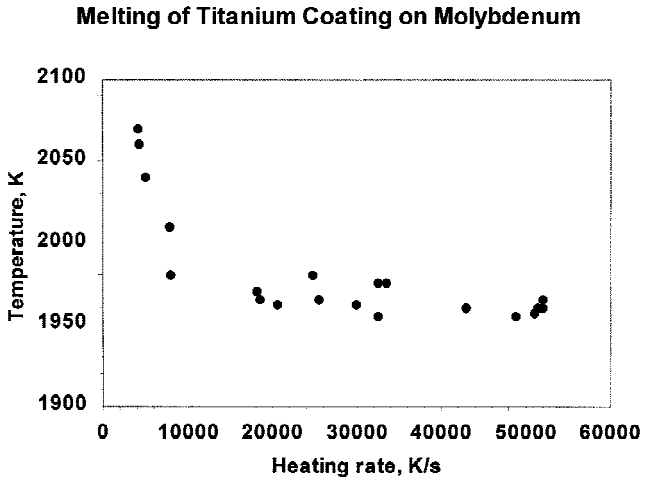

FIG. 1. Summary of the inception of melting for Ti coatings on Mo rod substrates plotted versus average heating rate. A clear trend is visible at heating rates less than approximately 10^4 Ks^{-1}, with coatings melting at significantly higher temperatures due to interdiffusion of Mo from the substrate into the Ti coating.

Ti specimens. Note that, for monolithic materials of this type the steady-state difference in temperature between the center and surface of a 1.58 mm radius Mo rod due to radiative losses from the surface is only approximately 3 K.[4] Other values from the literature are between 1941 and 1943 K. That the experimental value is higher than the accepted value might be indicative of oxygen or nitrogen in the films. For the materials of interest for study by this technique, an uncertainty of this size is acceptable.

The critical heating rate provides an experimental estimate of the effective diffusion rate for penetration of Mo into the Ti. The diffusion distance, x, for a constant heating rate, $\dot{T}$, is given by

$$x^2 = \frac{4A}{\dot{T}} \quad , \tag{1}$$

where

$$A = \int_{T_R}^{T_M} D_0 \exp[-Q/RT]\, dT \quad , \tag{2}$$

for constant heating rate from room temperature to the melting temperature. For Mo penetration into Ti, $D_0 = 0.24\ cm^2\ s^{-1}$ and $Q = 214.8\ kJ\ mol^{-1}$,[6] giving a value for $A = 5.2 \times 10^{-5}\ cm^2\ K\ s^{-1}$. For a heating rate of 1×10^4 $K\ s^{-1}$, $x = 1.4$ μm. However the experiments suggest that the penetration is about a factor of 10 greater than 1.4 μm, implying an experimental diffusion coefficient that is approximately 100 times larger than the published value. One possible explanation is a bulk diffusion coefficient in the evaporated thin films that is higher than the reported value due to a nonequilibrium (excess) concentration of point defects; highly defected crystalline structures are typical of thin films deposited on cooled substrates. The accelerated diffusion might also indicate the dominance of nonbulk diffusion paths, such as grain boundary diffusion.

B. Titanium(aluminum) alloy coatings

Specimens were fabricated with approximately 24 μm-thick Ti(Al) alloy coatings on Mo rods. These included six specimens with coatings of atomic fraction 0.19 ± 0.01 Al (2σ for all stated uncertainties) studied at heating rates between 7.0×10^4 and 9.5×10^4 $K\ s^{-1}$ and four specimens with coatings of atomic fraction 0.31 ± 0.01 Al studied at heating rates between 2.2×10^4 and 6.2×10^4 $K\ s^{-1}$. At these heating rates little penetration of Mo into the Ti(Al) coatings is expected. Figure 2 shows the radiance temperature and spectral emissivity recorded during a typical experiment along with the true temperature calculated from them. A short plateau of the true temperature, associated with the enthalpy of melting of the alloy coating, is observed. The flatness of the plateau is consistent with the small separation of the solidus and liquidus expected for this alloy (next section). For the Ti81Al19 specimens, the plateau occurs at 1939 ± 24 K. For the Ti69Al31 alloy specimens, the plateau occurs at 1925 ± 20 K.

C. Discussion of Ti and Ti(Al) alloy results

The experimental data available in the literature for the Ti–Al liquidus and solidus[7–9] are not considered reliable[10] because the melting temperatures that were measured for pure Ti in those papers are 20 to 50 K higher than the currently accepted value. The lack of reliable data results in uncertainty in the phase diagram. Liquidus and solidus lines obtained in thermodynamic assessments

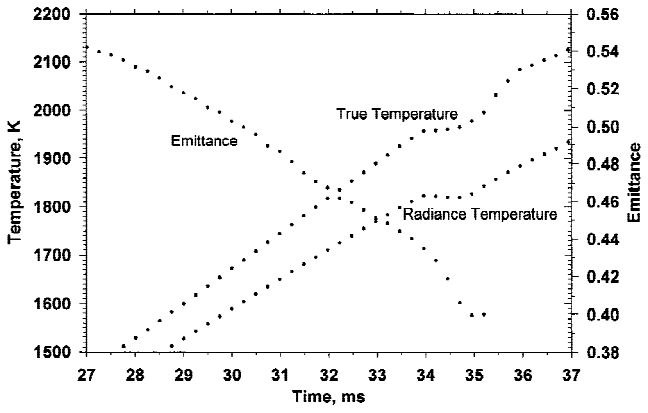

FIG. 2. Melting data for a 24 μm-thick, Ti81Al19 coating on a Mo substrate. The plot shows the radiance temperature recorded by the pyrometer (operating at 651 nm), the spectral emissivity measured by the polarimeter (operating at 633 nm), and the true temperature calculated from them using Planck's law. The difference in operating wavelengths for the two measurements leads to an error of less than 1 K for a Ti53Nb47 alloy.[4] The plateau in the true temperature is associated with the enthalpy of melting for the alloy.

predict behavior that ranges from a monotonic decrease with Al content[10–12] to a congruent maximum.[13,14] These features are shown in Fig. 3. The melting temperatures of the pure Ti, Ti81Al19, and Ti69Al31 alloy coatings measured in this study, because they decrease monotonically with Al content, are inconsistent with the congruent maximum. They are consistent with the liquidus (rather than solidus) data reported for higher Al concentrations[15] as seen in Fig. 3. Such is expected for rapid melting of an alloy.[4]

IV. RESULTS AND DISCUSSION: MELTING OF SUBSTRATES

A. Ti wires coated with Mo

Two experiments were conducted on Ti wire with 10 μm-thick Mo coating at heating rates of 5.5×10^4 K s^{-1}. Data from one experiment are shown in Fig. 4. The full melting plateau, associated with the latent heat of melting of the Ti wire, is obtained, which is not the case for uncoated specimens at these heating rates. The rapid decrease of the measured emissivity, indicating melting of the surface, and subsequent rapid failure (<2 ms later) of the specimen occur only after the end of the plateau. Thus, some thickness of the encapsulating solid Mo coating survives melting of the entire Ti wire. The relatively gradual change of slope toward the end of the plateau, as compared to the sharp corner at the start of the plateau, is likely a result of steadily increasing Mo concentration in the melt; this dissolution of the Mo coating ultimately leads to specimen failure. The plateau temperature of 1935 K (1933 K in the second experiment) is approximately 10 K below the melting temperature of Ti, which will be addressed later. However, for the materials of interest for study by this technique, an uncertainty even of this size is acceptable.

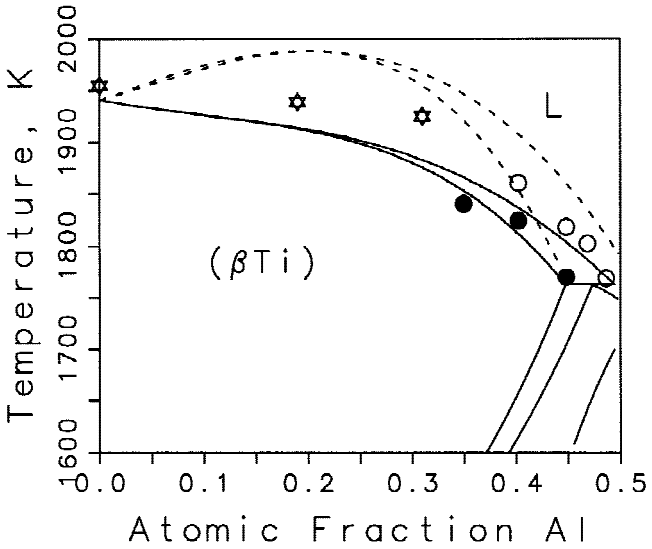

FIG. 3. Experimental data on the melting point for the Ti(Al) alloy coatings (stars) overlaid on the phase diagram calculated from thermodynamic assessments (solid,[10] dashed[14]) and DTA data[15] (liquidus, empty circle; solidus, filled circle).

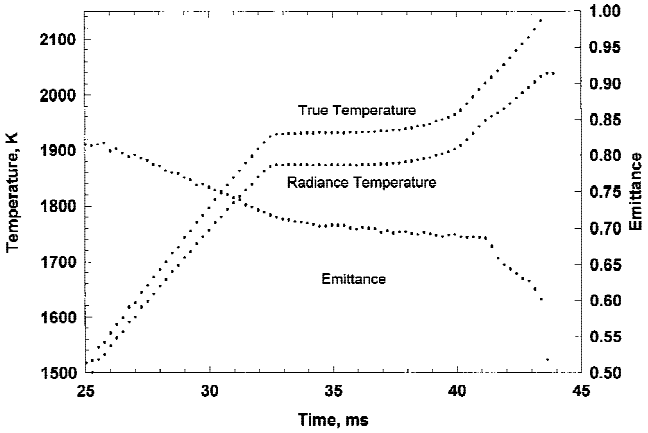

FIG. 4. Melting data for Ti rod coated with Mo. The plot shows the radiance temperature recorded by the pyrometer (operating at 651 nm), the spectral emissivity measured by the polarimeter (operating at 633 nm), and the true temperature calculated from them using Planck's law. The plateau in the true temperature is associated with the enthalpy of melting for the Ti. The rapid drop of the emissivity beyond 41 ms is associated with complete dissolution of the Mo coating that leads to failure of the now fully molten specimen.

B. Cr wires (high-oxygen) coated with W/Mo

The high-oxygen Cr was coated with approximately 1 μm W plus 15 to 20 μm Mo. Temperatures obtained with uncoated strips were approximately 50 K lower than those obtained for coated specimens, probably because of the high Cr vapor pressure over the Cr surfaces, and are excluded from this work. Heating experiments were performed on (1) six coated Cr rods at heating rates of 1×10^4 to 3×10^4 K s^{-1}, (2) four coated Cr strips at approximately 3×10^3 K s^{-1}, and (3) five Cr black-body tubes (uncoated) at 3×10^3 to 4×10^3 K s^{-1}, the tubes studied by pyrometry alone. A typical melting curve (Fig. 5) exhibits features not typical of a pure metal, viz., a discontinuous change in the slope of the temperature–time curves (approximately 1930 K) and a sloping plateau (approximately 2040 K inception). Similar results were obtained for all three types of specimens, ruling out interdiffusion as the cause of either event. With the coated rods and strips the slope change was observed at 1910 ± 15 K; the blackbody tubes yielded 1925 ± 10 K. The plateau inception was observed with the coated rods and strips at 2050 ± 20 K; the blackbody tubes yielded 2060 ± 10 K. Note that both the slope change and plateau inception obtained with the W/Mo coated Cr are 10 to 15 K lower than those obtained using the blackbody geometry. The value obtained for the melting point of Mo coated Ti was also 10 K lower than the accepted value (Sec. IV. A).

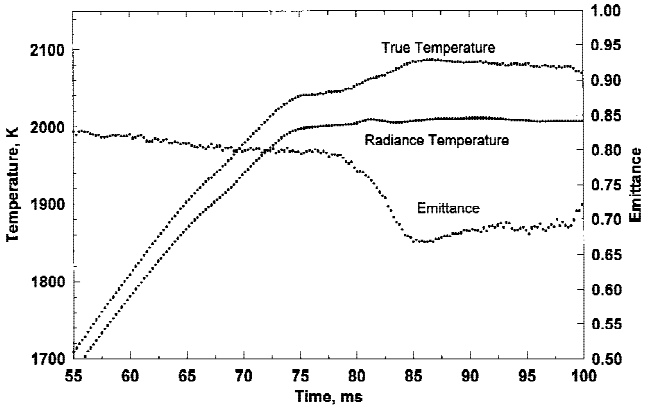

FIG. 5. Melting data for high-oxygen Cr rod coated with W and then Mo. The plot shows the radiance temperature recorded by the pyrometer (operating at 651 nm), the spectral emissivity measured by the polarimeter (operating at 633 nm), and the true temperature calculated from them using Planck's law. Note the deflection of the true temperature curve at 1930 K (67 ms) and plateau inception at 2040 K (74 ms). The emissivity drop at 79 ms indicates Cr has broken through the Mo coating.

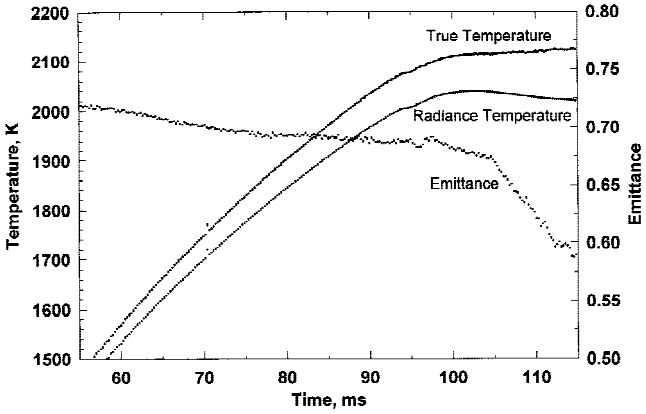

FIG. 6. Melting data for low-oxygen Cr rod coated with W and then Mo. The plot shows the radiance temperature recorded by the pyrometer (operating at 651 nm), the spectral emissivity measured by the polarimeter (operating at 633 nm), and the true temperature calculated from them using Planck's law. The main melting plateau (2120 K) is at the melting point of pure Cr, with melting of approximately 3% of the specimen (2070 K) at the Cr–O monotectic (discussed in Sec. IV. C).

The probable source of this discrepancy is the roughness of the coated surfaces, which persists through melting of the underlying substrate material; the underlying theory for analyzing the polarimeter data assumes a smooth surface. The roughness manifests as values of emittance (Figs. 4 and 5) that are nearly twice the 0.3 to 0.4 value typical of the spectral emissivity of a smooth Mo surface in this range of temperature and wavelength. To correct for this systematic measurement error, a +10 K correction is made, where noted, to the temperatures computed from the measured emissivities and radiance temperatures using Planck's law. Thus the corrected experimental temperatures for the slope change and plateau inception are 1920 ± 15 and 2060 ± 10 K, respectively.

C. Cr wires (low oxygen) coated with W/Mo

The low-oxygen Cr was prepared with rectangular and square cross sections of 3.2 mm × 1.6 mm and 1.6 × 1.6 mm, respectively. All were approximately 50 mm long. One side was polished on each specimen, and 1 μm W followed by 11 μm Mo was deposited on that side; the remaining three sides were coated with 0.3-μm W followed by 1 μm Mo. The pyrometer and polarimeter observed the side with the thick coating in all experiments. Results of a typical experiment are shown in Fig. 6. On the basis of the emissivity and true temperature behaviors, the Mo coating survived through partial melting of the Cr. A short "preplateau" of at most 1.5 ms in duration is distinguishable at a corrected temperature of 2080 ± 20 K, in most experiments, prior to the main plateau (Fig. 6). For constant input power, a prediction of the time required to fully melt the specimen is obtained by dividing the latent heat by the specific heat and heating rate prior to the plateau.[4] For Cr this is approximately 350 K divided by the heating rate which gives 35 ms at a heating rate of 1×10^4 K s^{-1}. The preplateau thus corresponds to melting of at most 4% of the specimen; it is discussed in the next section. The corrected temperature of the main plateau, at which the bulk of melting occurs (see Fig. 6), is 2115 ± 20 K from seven experiments. This temperature, 2115 ± 20 K, is the melting point of pure Cr.

D. Discussion of Cr results

A version of the Cr–O phase diagram from a selected source[17] is shown in Fig. 7. For the low-oxygen Cr (2.5×10^{-4} atomic fraction oxygen), the phase diagram predicts approximately 1% of the material should melt at the monotectic temperature (2073 K), with the rest melting, essentially, at the melting point of pure Cr (2133 K). The corrected temperatures of the preplateau and main plateau observed during melting of the low-oxygen Cr are consistent with the monotectic and the Cr melting point on the phase diagram, respectively. The fraction melted during the preplateau is also consistent with the prediction of the phase diagram.

For the high-oxygen Cr (0.005 atomic fraction oxygen), the phase diagram in Fig. 7 predicts approximately 1% of the material should melt at the eutectic temperature (1933 K) and approximately one-quarter of the material should melt at the monotectic temperature. Additional melting should occur as the temperature approaches the liquidus. Consistent with these predictions, the corrected slope-change and plateau-inception temperatures are quite close to the temperatures of the

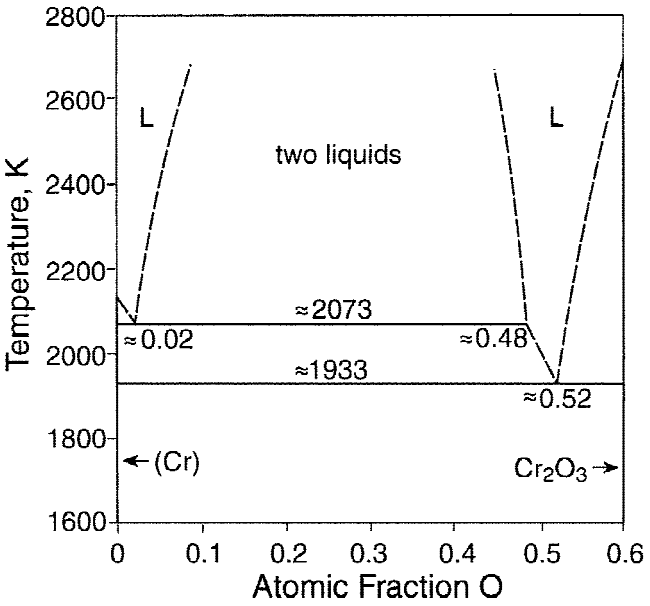

FIG. 7. Partial binary phase diagram for the Cr–O system.[17]

eutectic and the monotectic on the phase diagram, respectively, with a weaker signal at the slope change (eutectic).

Values selected in compilations for the melting temperature of pure Cr vary by approximately 50 K. Two graphical compilations of binary phase diagrams involving Cr with melting points for Cr of 2133 K[17] and 2136 K[16] are in reasonable agreement with the corrected value 2115 ± 20 K obtained in this work. Analytical descriptions of the free energy of pure Cr in thermodynamic computations of binary phase diagrams use a higher melting point of 2180 K,[18,19] inconsistent with the value obtained here. Phase diagrams for the Cr–O system from various sources include an approximately 90 K range of values for the monotectic temperature: 2073 K;[17] 2093 K;[16] 2130 K;[18] 2160 K.[19] [More recent thermodynamic based assessments,[17,18] added the Cr_3O_4 phase into the phase diagram. For this case, the eutectic [L → (Cr) + Cr_3O_4] replaces [L → (Cr) + Cr_2O_3] with only a small change in temperature.] The eutectic, monotectic, and pure Cr melting points of Ref. 17 (see Fig. 7) and Ref. 16 (for the eutectic) are consistent with the experimental data from both the high-oxygen and low-oxygen Cr specimens. Temperatures for the monotectic and pure Cr melting points obtained from the thermodynamic assessments[18,19] are significantly higher than the corresponding experimental values.

V. MODELING OF TEMPERATURE DISTRIBUTIONS IN COATED SPECIMENS

The heating rates, $\dot{T}$, in these experiments are sufficiently fast (1×10^4 to 5×10^4 K s^{-1}) that the specimens can be considered adiabatic; radiated power is only approximately 1% of the input power.[20] Since continuous current is used, the density of current, j, and thus the heat source term, $\dot{H} = \rho j^2$, would be uniform if the electrical resistivity, ρ, were uniform. As can be seen in Table I, the room-temperature resistivity of W and Mo are nearly the same, but that of Cr is more than twice as large and that of Ti is nearly eight times larger. However, using the temperature-dependent properties shown for Mo and Ti in Table II, by 2000 K the resistivity of Ti is only twice as large. Considering the two materials of the substrate (s) and coating (c), for specimen length much greater than radius, one can write

$$E = \rho_s j_s = \rho_c j_c \quad , \tag{3}$$

where E is the electrical field (i.e., the voltage/unit length) in the wire and currents are presumed uniform within both the coating and the substrate. The Joule source terms in the two media are therefore given by the following relationship:

$$\dot{H}_s = E j_s = \frac{E^2}{\rho_s} = \frac{\rho_c}{\rho_s}\dot{H}_c \quad \text{or} \quad \frac{\dot{H}_s}{\dot{H}_c} = \left[\frac{\rho_s}{\rho_c}\right]^{-1} \quad . \tag{4}$$

The ratio of the Joule source terms is therefore inverse the ratio of the electrical resistivities.

The heat balance to be solved in the wire can be written as

$$\frac{\partial h_\nu}{\partial t} = \frac{1}{r}\frac{\partial}{\partial r}\left[\kappa_\nu r \frac{\partial T}{\partial r}\right] + \dot{H}_\nu \quad \nu = \text{s or c} \quad , \tag{5}$$

where κ is the thermal conductivity and h_ν the volumetric enthalpy of phase ν. The time derivative of the enthalpy can also be written:

$$\frac{\partial h_\nu}{\partial t} = (c_p)_\nu \frac{\partial T}{\partial t} - L_\nu \frac{\partial g_s}{\partial t} \quad \nu = \text{s or c} \quad , \tag{6}$$

where c_p is the volumetric specific heat, L_ν the volumetric latent heat of fusion, g_s the volume fraction of solid, and T the temperature field. Continuity of the temperature at the substrate/coating interface has been assumed, and the latent heat (if remelting occurs) is released at the melting point. Using temperature-dependent thermal and electrical properties (Table II), Eqs. (5) and (6) have been solved using a simple 1-dimensional finite volume program based on an implicit

TABLE I. Room-temperature properties of bulk elements.[21]

	Resistivity, ρ (10^{-8} Ω m)	Conductivity, κ (W m^{-1} K^{-1})	Specific heat, c_p (10^6 J m^{-3} K^{-1})
Cr	12.9	93.9	3.22
W	5.65	177	2.59
Ti	42	22.4	2.35
Mo	5.2	139	2.52

TABLE II. Temperature-dependent properties[a] of bulk elements.[22]

	Resistivity, ρ (10^{-8} Ω m)	Conductivity, κ (W m^{-1} K^{-1})	Specific heat, c_p (10^6 J m^{-3} K^{-1})
Ti(300:1150) K	0.16 T	20.9–1.25 × 10^{-3} T	2.07 + 9.4 × 10^{-4} T
Ti(1150:2000) K	134 + 0.012 T	20.9–1.25 × 10^{-3} T[b]	1.79 + 9.4 × 10^{-4} T
Mo(300:2000) K	0.0205 T	146–3.48 × 10^{-2} T	2.38 + 6.6 × 10^{-4} T

[a]Room-temperature values obtained from the expressions are consistent with those given in Table I[21] except for the electrical resistivities,[22] which are both approximately 20% higher.
[b]Extrapolated from lower temperature data.

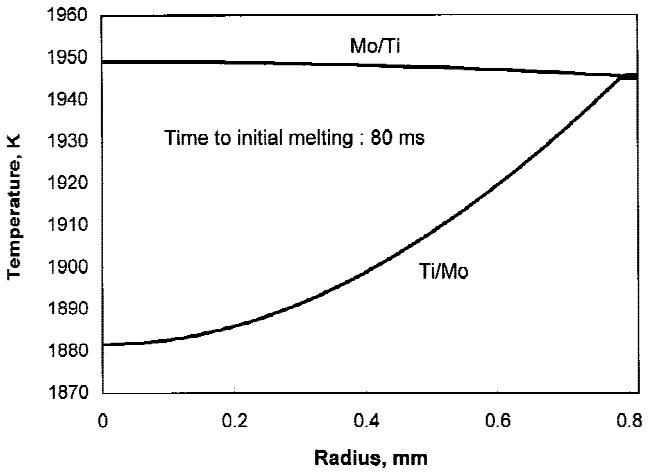

FIG. 8. Calculations of the temperature distributions in specimens composed of a coating of Ti on a Mo rod (Mo/Ti) and for a coating of Mo on a Ti rod (Ti/Mo). The temperature distributions are shown at approximately 80 ms, with the coating 24-μm thick and the rod 1.59 mm in diameter in both cases. Power inputs are such that the temperature at some location in the Ti has just reached the melting point of Ti (1945 K).

scheme and a temperature recovery method (i.e., the temperature of a remelting volume element is held at the melting point until the corresponding value $g_{s,v}$ is equal to zero). As the process is nearly adiabatic during the very short heating times, the calculations were performed with a homogeneous Neumann condition at the surface of the coating.

The results of calculations of temperature distributions for a coating of Ti on a Mo rod and for a coating of Mo on a Ti rod are shown in Fig. 8. The input power is such that the inception of melting occurs at approximately 80 ms, with the coating 24-μm thick and the rod 1.59 mm in diameter in both cases. The calculations represent the temperature profile when the temperature at a location in the Ti first reaches the melting point (1945 K). The Mo heats more rapidly than the Ti because the ratio of the heat source term and the specific heat is larger for Mo than for Ti. For this reason, the Ti first melts at the Ti/Mo interface. For the case of a Ti rod coated with Mo, most of the heating occurs in the Mo coating and thermal diffusion limitations result in a rather nonuniform temperature field. The temperature difference between the surface of the coating and the center of the wire is approximately 60 K. In contrast, for a Mo rod is coated with Ti, most of the heating occurs in the Mo wire and fast thermal diffusion through the thin coating results in a variation of only 3 K across the entire specimen (see Fig. 8).

On the basis of these calculations, experiments with the Ti coating on the Mo rod should be most accurate for measuring the melting point of Ti. Even though the Ti at the interface begins to melt prior to that on the surface viewed by the instruments, the temperature change across the thin coating is much less than 1 K. There is no reason to expect a systematic error with specimens of this geometry.

For the Mo coating on the Ti rod specimens, the temperature rise across the Mo coating is also $\ll 1$ K when the Ti at the interface begins to melt (Fig. 8). However, as further heating and melting occur, a temperature gradient will form in the liquid (absent convection). The Mo coating, and the molten Ti adjacent to it, will rise to temperatures above the melting point of Ti, even while the inner region of the Ti rod is still in the process of melting. The increase in temperature evident in the latter part of the Ti melting plateau (Fig. 4) might be a manifestation of this, though Mo and Ti interdiffusion is also consistent with this increase. This effect is significantly smaller for the Mo-coated Cr specimens due to the similarity of the Mo and Cr resistivities (Table I) and the thinner coatings.

VI. UNCERTAINTIES

The uncertainties associated with measurements obtained from the pyrometer and polarimeter in this approximate temperature range have been noted previously.[4] In those results, uncertainty associated with the pyrometry was 7 K (2σ); uncertainty associated with the polarimetry was 2% (5 K). The resulting combined uncertainty was 10 K. The scatter of the data for the Ti coatings on Mo as well as the Mo coatings on Ti are consistent with this 10 K uncertainty. The scatter in the data from the Ti81Al19- and Ti69Al31-coated specimens, noted to be 24 and 20 K, respectively, are significantly larger (all uncertainties in this work are 2σ). The source of this additional scatter is believed to include

some contribution from actual composition variation of the specimens. On the basis of these data, total measurement uncertainties of 25 and 22 K apply to these melting temperatures. The scatter in the results for the melting point of low-oxygen Cr, 20 K, yields a total measurement uncertainty of 23 K, including instrumental uncertainties, for the melting point of Cr.

VII. CONCLUSIONS

The results of two geometrically identical but fundamentally different types of pulsed heating experiments have been described for measuring melting temperatures. Both types of experiment use coated substrate specimens; the use of substrate materials with melting temperatures higher (lower) than that of the coating was shown to yield the melting temperature of the coating (substrate) material. Experiments with Ti coatings on Mo rods studied at different heating rates were used to quantify the experimental conditions required to overcome interdiffusion-induced artifacts. The results of studies with the Ti coatings on Mo substrates, as well as with Ti substrates coated with Mo, demonstrated the accuracy to be expected from such experiments. Results from Ti(Al) alloy coatings yielded melting temperature data helpful for understanding a portion of the Ti–Al phase diagram, demonstrating that a congruent maximum does not exist in the Ti-rich side. Measurement of the melting point of Cr through the use of coated Cr specimens yielded the melting point of Cr (2115 ± 20 K), demonstrating that the melting points used in thermodynamic assessments are at least 50 K too high. A monotectic and a eutectic temperature on the Cr–O phase diagram were also obtained.

REFERENCES

1. A. Cezairliyan, M.S. Morse, H.A. Berman, and C.W. Beckett, J. Res. Natl. Bur. Stand. (U.S.) **74A,** 65 (1970).
2. A. Cezairliyan, J. Res. Natl. Bur. Stand. (U.S.) **75C,** 7 (1971).
3. A. Cezairliyan, S. Krishnan, and J.L. McClure, Int. J. Thermophys. **17,** 1455 (1996).
4. D. Basak, W.J. Boettinger, D. Josell, S.R. Coriell, J.L. McClure, S. Krishnan, and A. Cezairliyan, Acta Mater. **47,** 3147 (1999).
5. R.M. Waterstrat, Natl. Inst. Stand. Tech. Rep. NISTIR 88-3856, 1988.
6. *Metals Reference Book*, 5th ed., edited by C.J. Smithells (Butterworths, London, United Kingdom, 1976), p. 879, tracer diffusion coefficients for Mo in Ti.
7. H.R. Ogden, D.J. Maykuth, W.L. Finlay, and R.J. Jaffee, Trans. AIME **191,** 1150 (1951).
8. E.S. Bumps, H.D. Kessler, and M. Hansen, Trans. AIME **194,** 609 (1952).
9. I.I. Kornilov, E.N. Pylaeva, and M.A. Volkova, Izvest. Akad. Nauk SSSR, Otd. Khim. Nauk **7,** 771 (1956).
10. U.R. Kattner, J-C. Lin, and Y.A. Chang, Metall. Trans. A **23A,** 2081 (1992).
11. F. Zhang, S.L. Chen, Y.A. Chang, and U.R. Kattner, Intermetallics **5,** 471 (1997).
12. I. Ohnuma, Y. Fujita, H. Mitsui, K. Ishikawa, R. Kainuma, and K. Ishida, Acta Mater. **48,** 3133 (2000).
13. J.L. Murray, Metall. Trans. A **19A,** 243 (1998).
14. N. Saunders, in *COST 507*, edited by I. Ansara, A.T. Dinsdale, and M.H. Rand (European Communities, Luxembourg, 1998), Vol. 2, pp. 89–95.
15. J.C. Mishurda and J.H. Perepezko, in *Microstructure—Property Relationships in Titanium Aluminides and Alloys*, edited by Y.W. Kim and R.R. Boyer (TMS, Warrendale, PA, 1991), pp. 3–30.
16. *Binary Alloy Phase Diagrams*, 2nd ed., edited by T.B. Massalski (ASM, Materials Park, OH, 1990), pp. 1304–1305.
17. B. Predel, in *Landolt-Börnstein, New Series: Phase Equilibria, Crystallographic and Thermodynamic Data of Binary Alloys*, edited by O. Madelung (Springer, Berlin, Germany, 1994), Gr. IV, Vol. 5, Subvol. d, pp. 49–50.
18. J.R. Taylor and A.T. Dinsdale, Z. Metallkde. **81,** 354 (1990).
19. M. Kowalski and P.J. Spencer, CALPHAD **19,** 229 (1995).
20. D. Basak, U.R. Kattner, J.L. McClure, D. Josell, and A. Cezairliyan, Int. J. Thermophys. **21,** 913 (2000).
21. *Handbook of Chemistry and Physics*, 68th ed. (CRC Press, Boca Raton, FL, 1987–88).
22. *Thermophysical Properties of High Temperature Solid Materials*, edited by Y.S. Touloukian (Macmillan, New York, 1967), Vol. 1.